ENAE464 - 0202

Lab02: Pressure Drag and Lift on an Airfoil Model

Due on February 27th, 2026 at 11:59 PM

Dr. Silbaugh, 02:00 PM

Mikołaj Kostrzewa & Vai Srivastava

Experiment Performed: February 20th, 2026
Report Submitted: February 27th, 2026

February 27$^{\text{th}}$, 2026

Enclosed is the technical report for the *Pressure Drag and Lift on an Airfoil Model* laboratory experiment. This report presents the experimental methodology, results, and analysis of aerodynamic characteristics observed on the surface of a scale model of a NACA airfoil, including lift coefficient and drag coefficient distributions, aerodynamic force analyses, and comparison with published NACA data.
Please feel free to contact us with any questions regarding the contents of this report.

Respectfully,
Mikołaj Kostrzewa & Vai Srivastava

Contents

Figures

Tables

Listings

1 Abstract

The pressure distribution, lift, and drag characteristics of a NACA 4412 airfoil model were investigated experimentally in a 12 in × 12 in open-circuit wind tunnel at a freestream velocity of $U_\infty = 32.05\,\mathrm{m/s}$ and a chord Reynolds number of $Re \approx 6.58 \times 10^5$. Surface pressures were sampled at fourteen tap locations across both the upper and lower surfaces using a 16-channel differential pressure data acquisition system, and measurements were repeated at twenty-one angles of attack spanning $-20^\circ \leq \alpha \leq 20^\circ$ in 2° increments. Pressure coefficients were integrated via the trapezoidal rule to yield normal and axial force coefficients, which were resolved into lift and pressure drag coefficients in the wind axis. The experimental lift curve exhibited a maximum lift coefficient of $C_{L,\max} = 0.527$ at a stall angle of $\alpha_s = 8^\circ$. These values are substantially lower than the published XFoil polar for this airfoil at $Re = 1 \times 10^6$, which predicts $C_{L,\max} = 1.671$ at $\alpha_s = 16.25^\circ$. The discrepancies are attributed primarily to the coarse spatial resolution of the pressure tap array, which fails to resolve the leading-edge suction peak, and to the lower experimental Reynolds number, which promotes earlier laminar separation. Despite the quantitative differences, the experiment correctly captures the qualitative aerodynamic trends: a linear lift curve in the attached-flow regime, a characteristic low-drag bucket in the drag polar, and a rapid drag rise coinciding with flow separation.

2 Introduction

When a body moves through a fluid, the fluid exerts a resultant aerodynamic force that can be decomposed into two orthogonal components relative to the direction of the oncoming flow: the *drag* force F_D, acting parallel to the flow, and the *lift* force F_L, acting perpendicular to it. For a streamlined body such as an airfoil, both components arise from the spatial distribution of surface pressure and viscous shear stress, and both vary strongly with the *angle of attack* α — the angle between the airfoil chord line and the freestream velocity vector U_∞.

The NACA 4412 profile is a classical cambered airfoil from the National Advisory Committee for Aeronautics four-digit series [1]. Its designation encodes a maximum camber of 4 % chord located at 40 % chord, and a maximum thickness of 12 % chord. Its favourable pressure-recovery characteristics and relatively gentle stall behaviour make it a common benchmark in both computational and experimental aerodynamics courses.

In this experiment, a scale model of the NACA 4412 was instrumented with fourteen surface pressure taps and tested in a low-speed wind tunnel across a wide range of angles of attack. The primary objectives were:

1. to measure the surface pressure distribution $C_p(x/c)$ at each angle of attack and examine how it evolves with incidence;
2. to integrate these distributions to obtain lift and pressure drag coefficients as functions of α;
3. to identify the stall angle and maximum lift coefficient from the experimental C_L–α curve; and
4. to compare all experimental results against the published XFoil polar for the same airfoil at $Re = 1 \times 10^6$, identifying and explaining any discrepancies.

The experiment illustrates several fundamental concepts in aerodynamics: the relationship between surface pressure and aerodynamic force, the role of leading-edge suction in generating lift, the distinction between pressure drag and total drag, and the influence of Reynolds number and measurement resolution on the accuracy of pressure-integrated force estimates. The remainder of this report is organised as follows. Section 3 describes the wind tunnel facility, instrumentation, and data-reduction procedure. Section 4 presents the measured pressure distributions, force coefficients, and the stall characteristics derived from them. Section 5 compares the experimental results against published NACA data and discusses the sources of discrepancy. Section 6 summarises the principal findings and conclusions.

3 Experimental Apparatus and Procedures

3.1 Experimental Apparatus

Experiments were conducted in the 12 in × 12 in open-circuit wind tunnel located in the Thermal-Fluids Instructional Laboratory. The rectangular test section measures 12 in in height, 12 in in width, and 24 in in length, with a maximum achievable flow speed of approximately 40 m/s. Fan speed is regulated by a variable-frequency drive, with measurements taken at a fixed frequency setting assigned to each group (30 Hz, 35 Hz, or 40 Hz).

The test model is a two-dimensional NACA 4412 airfoil with a chord length of $c = 10$ cm. The model spans the full 12 in width of the test section, enforcing a nominally two-dimensional flow field. The angle of attack α is adjusted manually via a rotation mechanism mounted to the tunnel sidewall, shown below in Figure 3.1.1, which allows the model to be set at discrete angles throughout the sweep.

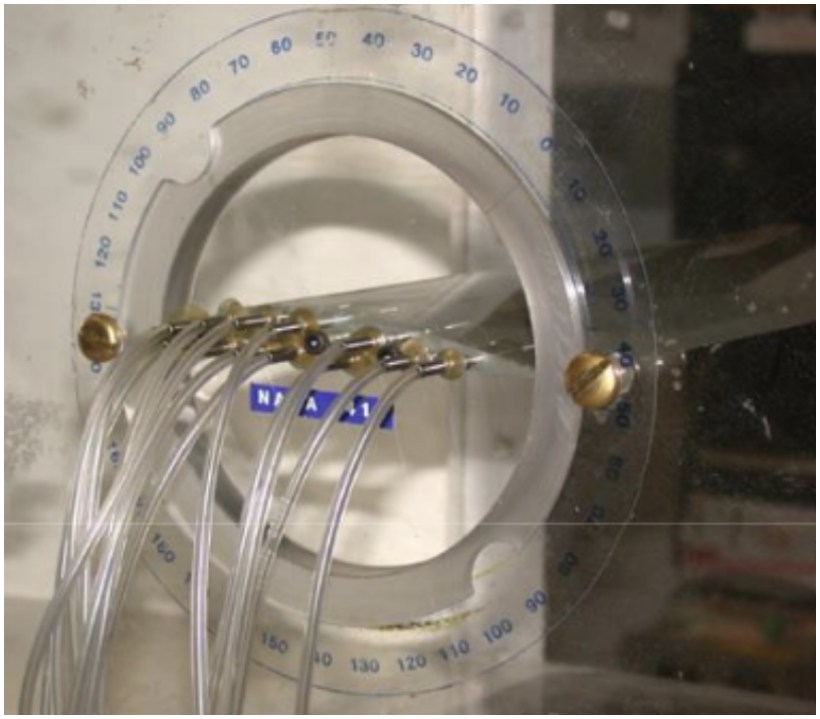

Figure 3.1.1: Airfoil with Attached Pitot Tubes in the Wind Tunnel Test Section

Fourteen static pressure taps are distributed across both surfaces of the airfoil. Eight taps are located on the upper surface at non-dimensional chord positions $x/c = 0.80$, 0.60, 0.40, 0.30, 0.20, 0.10, 0.05, and 0.00 (the leading edge), and six taps are on the lower surface at $x/c = 0.05$, 0.15, 0.25, 0.35, 0.50, and 0.65. The complete tap coordinates are listed in Table 8.1.2 in the Appendix.

All fourteen surface taps are connected to a 16-channel differential pressure data acquisition system (DSA). The DSA records all static pressures relative to the atmospheric reference: Channel 1 is left open to the atmosphere and serves as the gauge reference (P_{atm}), and Channels 2 through 15 are connected to pressure Taps 1 through 14 respectively. An additional static pressure tap is installed on the floor of the wind tunnel immediately upstream of the test section; this tap is connected to Channel 16 and measures the tunnel static pressure P_{static}, which is used together with the atmospheric reference to determine the freestream dynamic pressure.

3.2 Operating Technique

Prior to beginning the angle-of-attack sweep, the freestream velocity was established and verified. With the airfoil set to $\alpha = 0°$, the pressure at Tap 8 (Channel 9) — which corresponds to the leading-edge stagnation point at zero incidence — and the tunnel static pressure at Channel 16 were recorded simultaneously. The freestream dynamic pressure was then computed as

$$q_\infty = P_{\text{atm}} - P_{\text{static}} = P_{\text{Ch. 1}} - P_{\text{Ch. 16}}, \tag{3.2.1}$$

and the corresponding freestream velocity was obtained from $U_\infty = \sqrt{2q_\infty/\rho}$, where ρ is the ambient air density. This quantity was verified to remain consistent to within 3 % across all subsequent measurement points, confirming that the tunnel speed was nominally constant throughout the sweep.
Pressure data were then acquired at a minimum of ten angles of attack spanning the range $-12° \le \alpha \le 18°$. At each angle, the airfoil was held stationary while the DSA simultaneously sampled all sixteen channels, and the resulting pressure array was saved to the acquisition computer before proceeding to the next angle. Angles were incremented in steps of 2°, providing sufficient resolution to identify the onset of stall. Care was taken at each setting to allow the flow to reach a steady state before recording, and the model angle was read directly from the protractor scale visible in Figure 2 of the lab handout.
The recorded gauge pressures were subsequently post-processed to yield the pressure coefficient at each tap location,

$$C_p = \frac{P - P_\infty}{q_\infty} = \frac{P_{\text{tap}} - P_{\text{Ch. 16}}}{q_\infty}, \tag{3.2.2}$$

where $P_\infty = P_{\text{Ch. 16}}$ is the tunnel static pressure. Normal and axial force coefficients were obtained by numerically integrating the C_p distributions over the respective tap x/c and y/c coordinates using the trapezoidal rule, and these were subsequently resolved into lift and pressure drag coefficients in the wind axis via

$$C_L = C_n \cos(\alpha) - C_a \sin(\alpha)\,, \tag{3.2.3}$$

$$C_D = C_n \sin(\alpha) + C_a \cos(\alpha)\,. \tag{3.2.4}$$

4 Results

4.1 Incoming Wind Tunnel Airflow

The freestream dynamic pressure q_∞ was obtained from the pitot-static system by taking the difference between the atmospheric reference port (DSA Channel # 1) and the tunnel static pressure port (DSA Channel # 16):

$$q_\infty = P_{\text{atm}} - P_{\text{static}} = 629.15\,\text{Pa} \tag{4.1.1}$$

This value was consistent to within 3 % across all angles of attack, confirming that the tunnel speed remained nominally constant throughout the sweep.
The freestream velocity was recovered from the definition of dynamic pressure, $q_\infty = \frac{1}{2}\rho U_\infty^2$, using standard sea-level air density $\rho = 1.225\,\text{kg/m}^3$:

$$U_\infty = \sqrt{\frac{2q_\infty}{\rho}} = \sqrt{\frac{2 \times 629.15\,\text{Pa}}{1.225\,\text{kg/m}^3}} = 32.05\,\frac{\text{m}}{\text{s}} \tag{4.1.2}$$

The chord Reynolds number was then computed as

$$Re = \frac{\rho\, U_\infty\, c}{\mu} = \frac{1.225\,\text{kg/m}^3 \times 32.05\,\text{m/s} \times 0.3\,\text{m}}{1.789 \times 10^{-5}\,\text{Pa s}} = 6.58 \times 10^5 \tag{4.1.3}$$

where $c = 0.3\,\mathrm{m}$ is the airfoil chord length and $\mu = 1.789 \times 10^{-5}\,\mathrm{Pa\,s}$ is the dynamic viscosity of air at standard conditions. The resulting Reynolds number of $Re \approx 6.6 \times 10^5$ places the flow in the transitional regime, consistent with the expected behaviour of a NACA 4412 airfoil at low-speed wind tunnel conditions.

4.2 Coefficient of Pressure

Table 4.2.1: Pressure Coefficient on Both Upper and Lower Airfoil Surfaces vs. Angle of Attack

`./outputs/text/integrated_cp_table.csv`

AoA (α)	$C_{P,\mathrm{Upper}}$	$C_{P,\mathrm{Lower}}$
-20.0	-0.049673	-0.208545
-18.0	-0.062035	-0.196348
-16.0	-0.078238	-0.180838
-14.0	-0.076766	-0.165781
-12.0	-0.081161	-0.167515
-10.0	-0.072895	-0.186576
-8.0	-0.043732	-0.189727
-6.0	-0.072018	-0.080524
-4.0	-0.140837	-0.046457
-2.0	-0.196104	-0.018809
0.0	-0.232687	0.000225
2.0	-0.308824	0.028311
4.0	-0.35379	0.049968
6.0	-0.4385	0.070743
8.0	-0.47102	0.072431
10.0	-0.449086	0.08427
12.0	-0.436332	0.08388
14.0	-0.437749	0.087143
16.0	-0.330166	0.039478
18.0	-0.339066	0.04576
20.0	-0.355917	0.053332

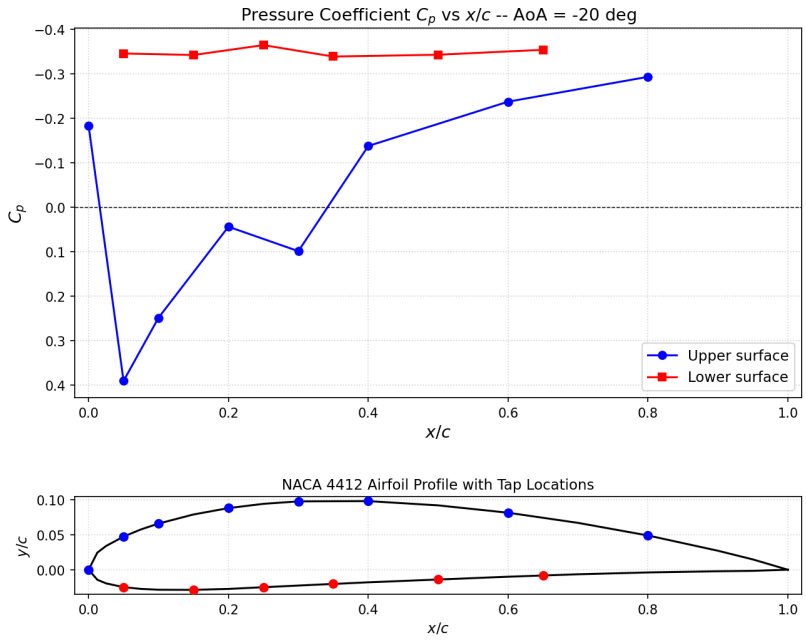

Figure 4.2.1: Pressure Coefficient C_p vs. Non-Dimensional Distance x/c for $-20\,^\circ$ Angle of Attack

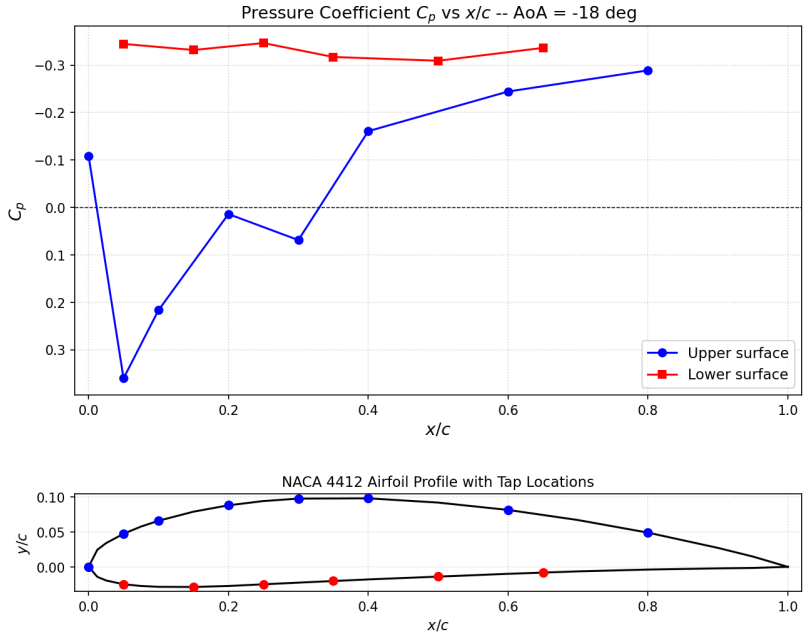

Figure 4.2.2: Pressure Coefficient C_p vs. Non-Dimensional Distance x/c for $-18\,^\circ$ Angle of Attack

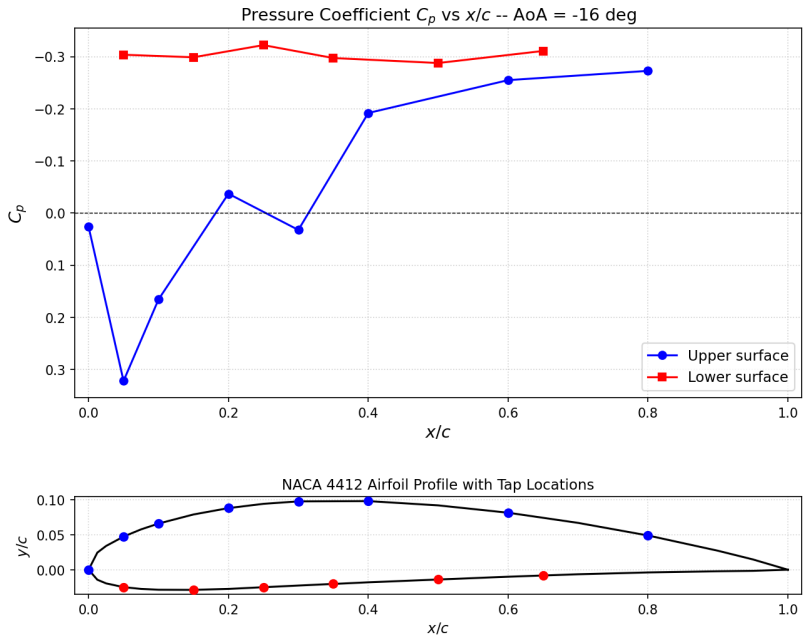

Figure 4.2.3: Pressure Coefficient C_p vs. Non-Dimensional Distance x/c for $-16\,^\circ$ Angle of Attack

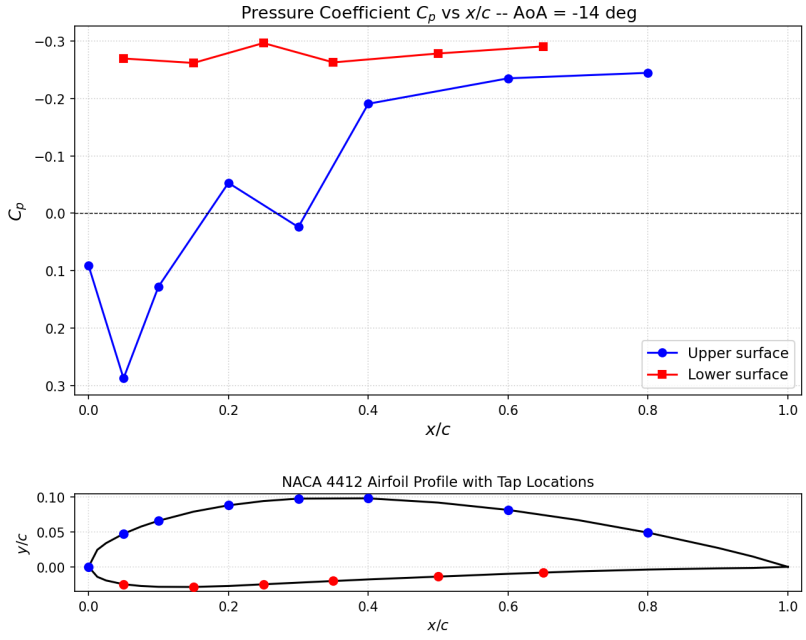

Figure 4.2.4: Pressure Coefficient C_p vs. Non-Dimensional Distance x/c for $-14\,^\circ$ Angle of Attack

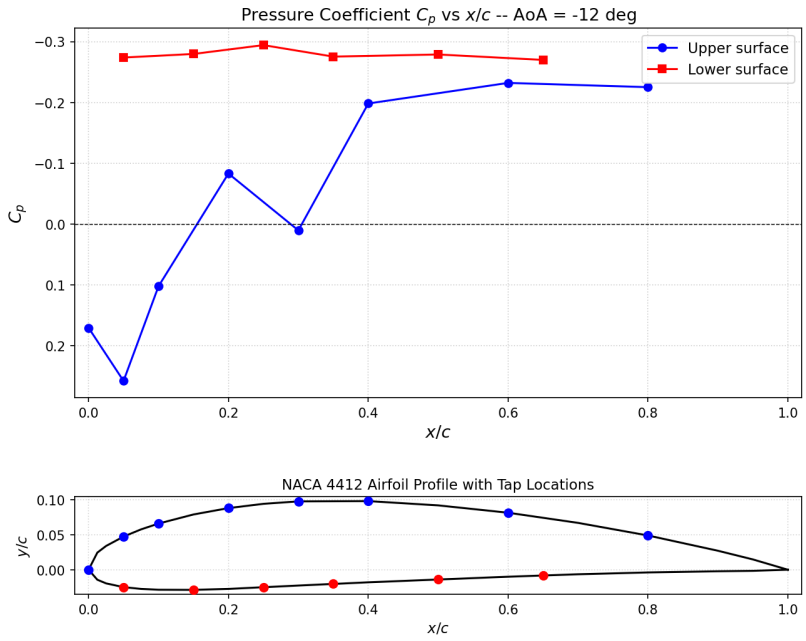

Figure 4.2.5: Pressure Coefficient C_p vs. Non-Dimensional Distance x/c for $-12\,^\circ$ Angle of Attack

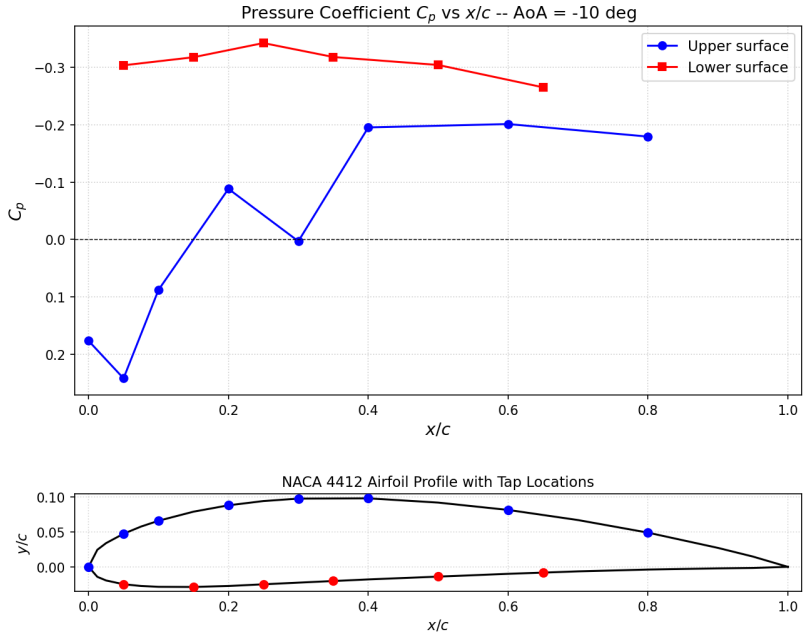

Figure 4.2.6: Pressure Coefficient C_p vs. Non-Dimensional Distance x/c for $-10\,^\circ$ Angle of Attack

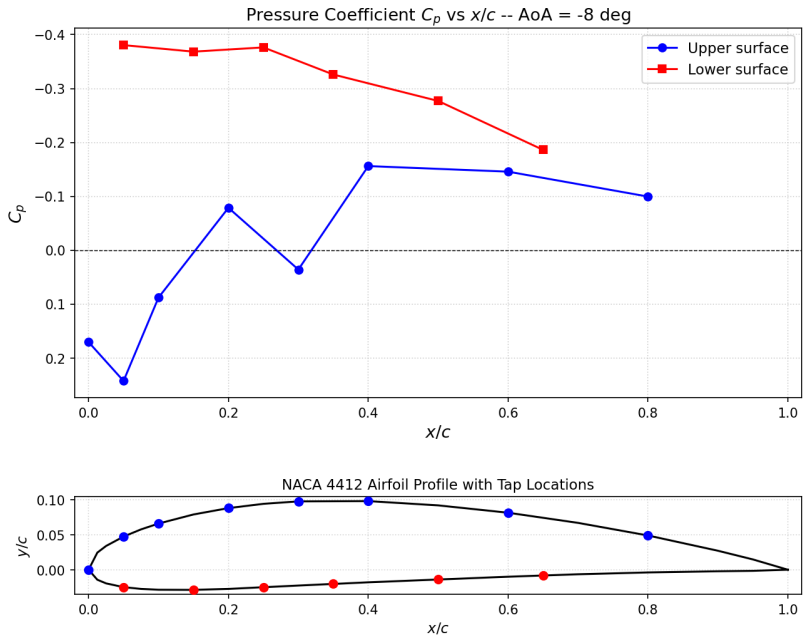

Figure 4.2.7: Pressure Coefficient C_p vs. Non-Dimensional Distance x/c for -8° Angle of Attack

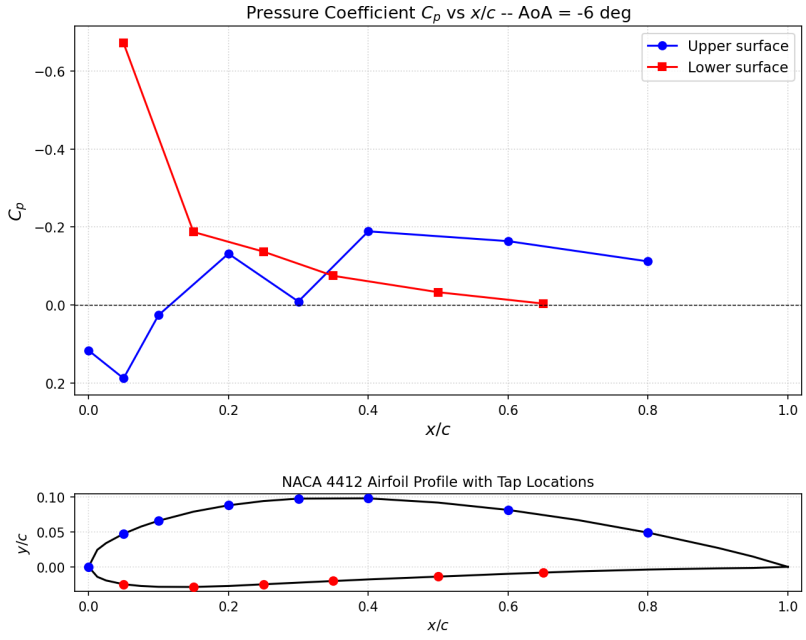

Figure 4.2.8: Pressure Coefficient C_p vs. Non-Dimensional Distance x/c for -6° Angle of Attack

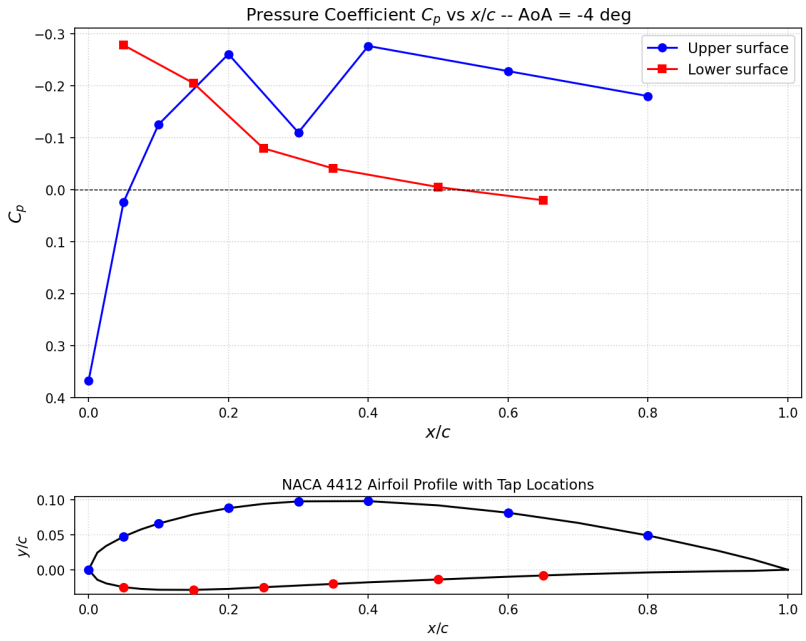

Figure 4.2.9: Pressure Coefficient C_p vs. Non-Dimensional Distance x/c for -4° Angle of Attack

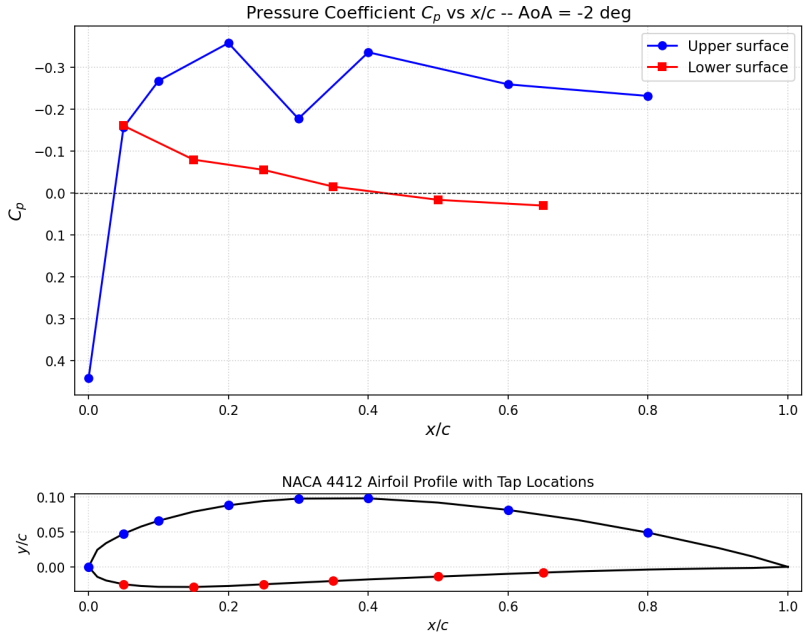

Figure 4.2.10: Pressure Coefficient C_p vs. Non-Dimensional Distance x/c for -2° Angle of Attack

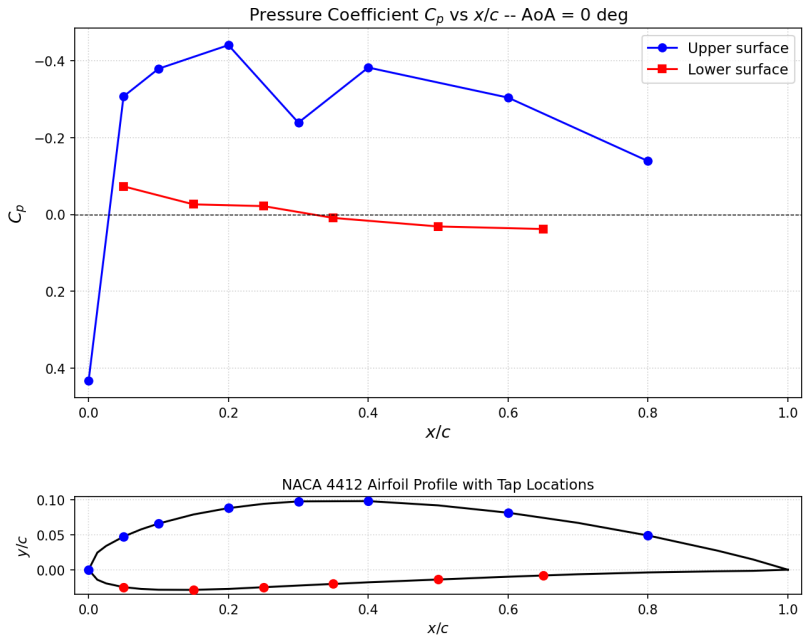

Figure 4.2.11: Pressure Coefficient C_p vs. Non-Dimensional Distance x/c for $0\,^\circ$ Angle of Attack

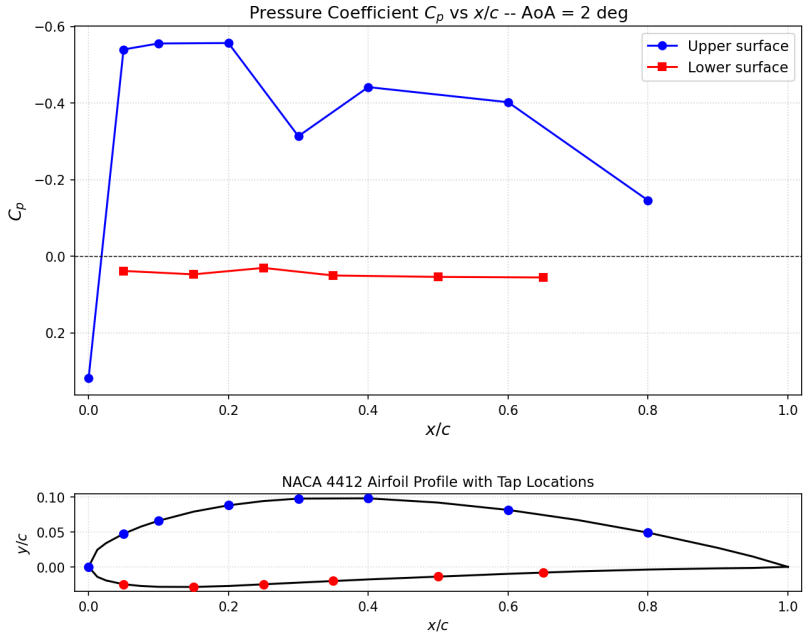

Figure 4.2.12: Pressure Coefficient C_p vs. Non-Dimensional Distance x/c for $2\,^\circ$ Angle of Attack

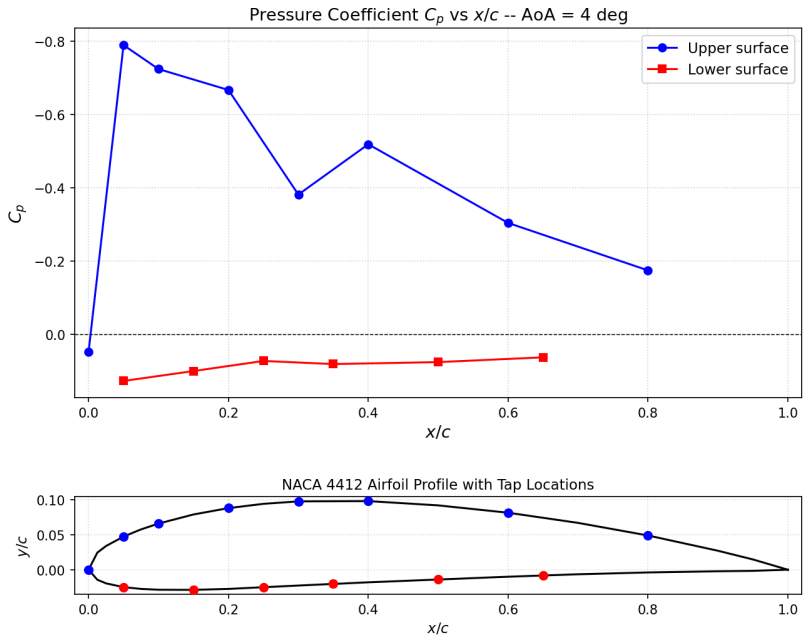

Figure 4.2.13: Pressure Coefficient C_p vs. Non-Dimensional Distance x/c for $4\,^\circ$ Angle of Attack

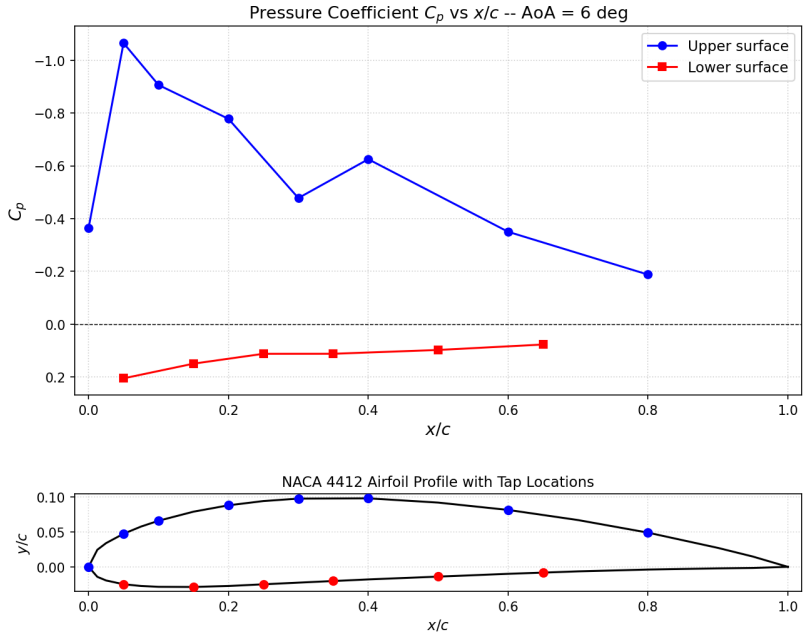

Figure 4.2.14: Pressure Coefficient C_p vs. Non-Dimensional Distance x/c for $6\,^\circ$ Angle of Attack

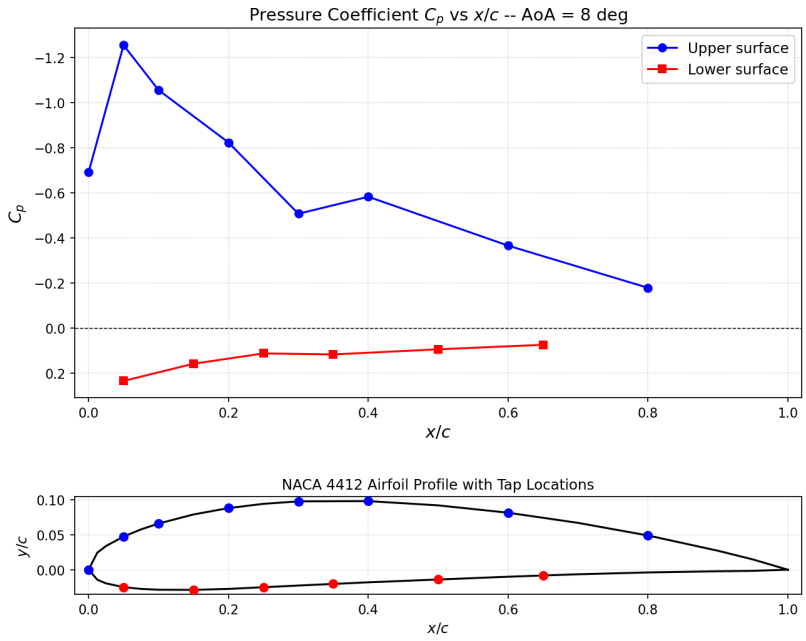

Figure 4.2.15: Pressure Coefficient C_p vs. Non-Dimensional Distance x/c for 8° Angle of Attack

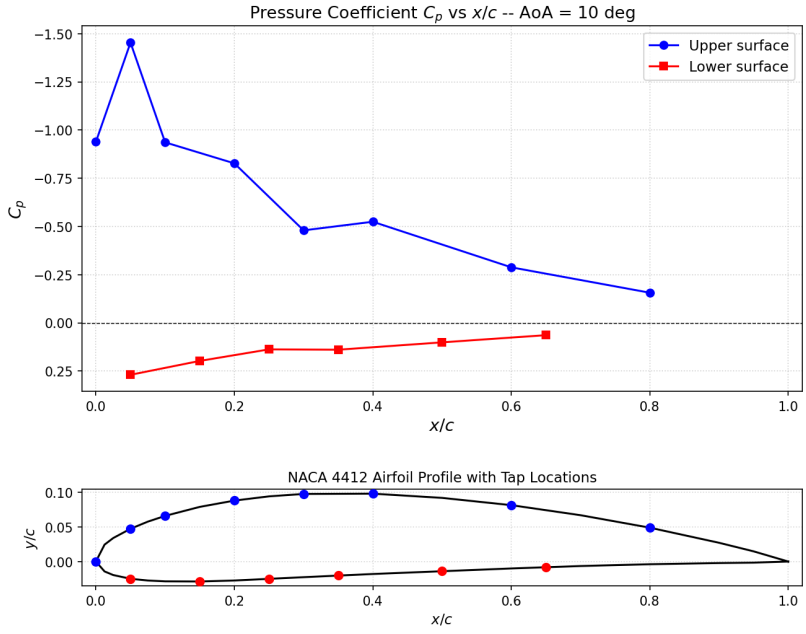

Figure 4.2.16: Pressure Coefficient C_p vs. Non-Dimensional Distance x/c for 10° Angle of Attack

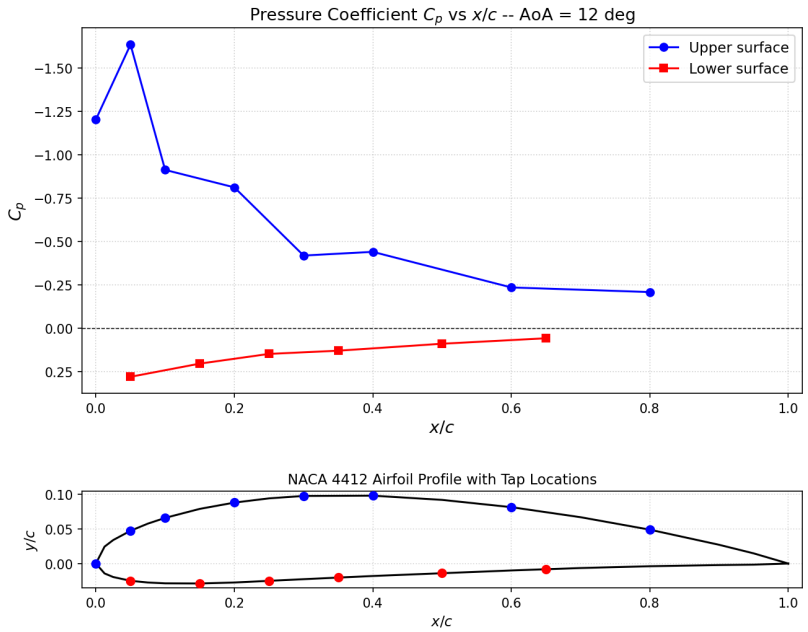

Figure 4.2.17: Pressure Coefficient C_p vs. Non-Dimensional Distance x/c for 12° Angle of Attack

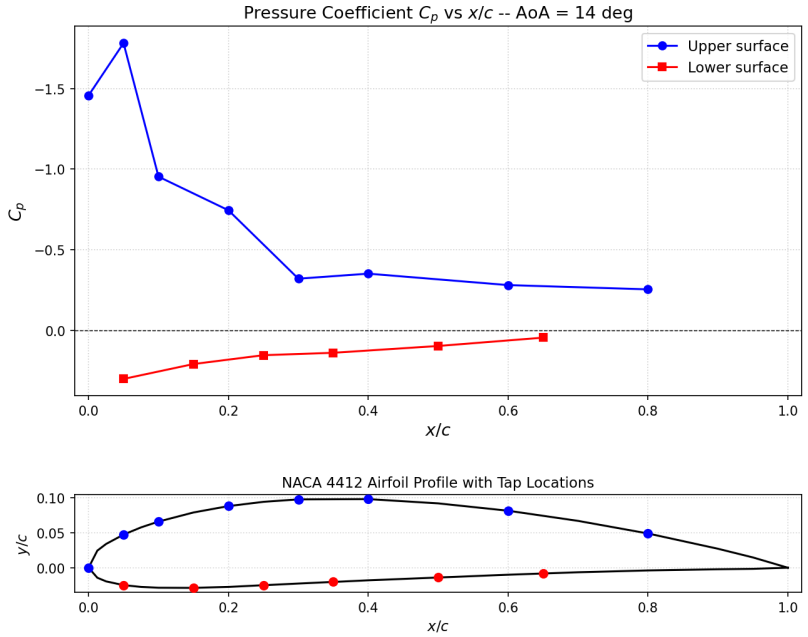

Figure 4.2.18: Pressure Coefficient C_p vs. Non-Dimensional Distance x/c for 14° Angle of Attack

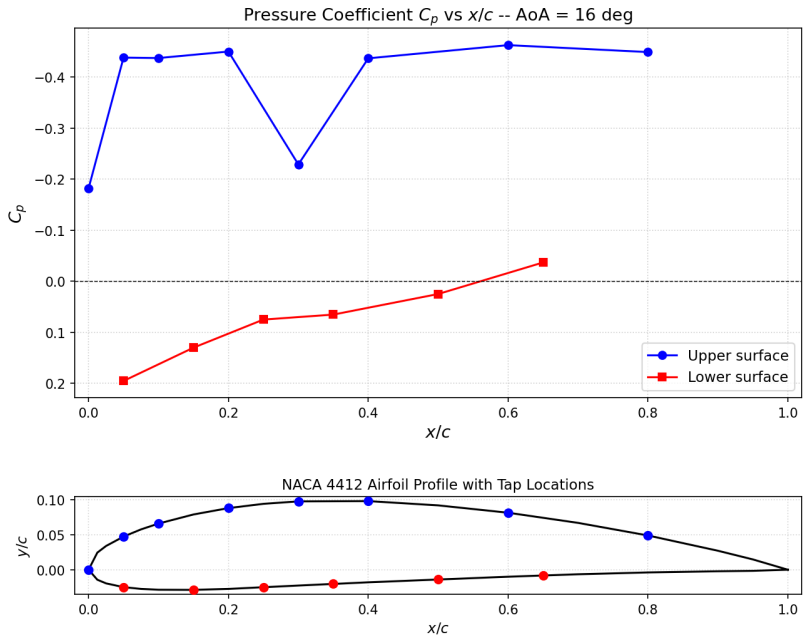

Figure 4.2.19: Pressure Coefficient C_p vs. Non-Dimensional Distance x/c for 16° Angle of Attack

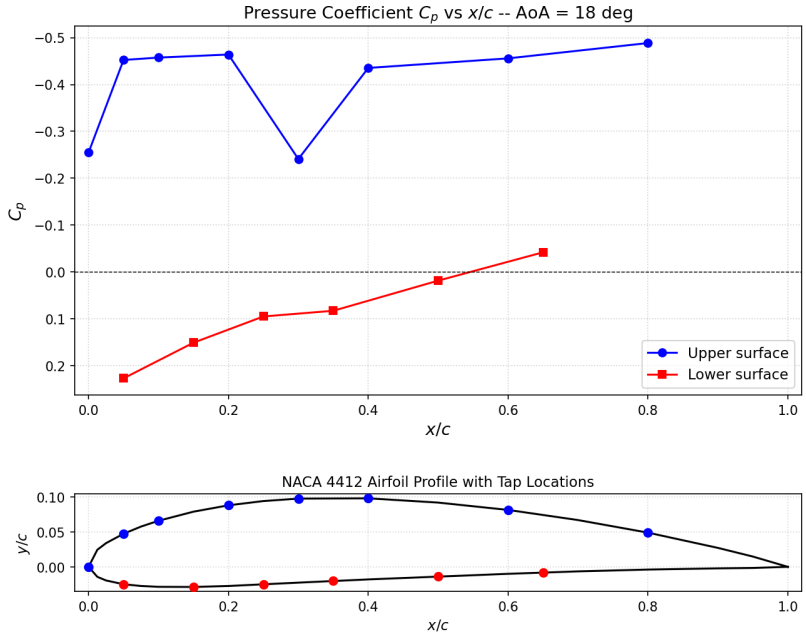

Figure 4.2.20: Pressure Coefficient C_p vs. Non-Dimensional Distance x/c for 18° Angle of Attack

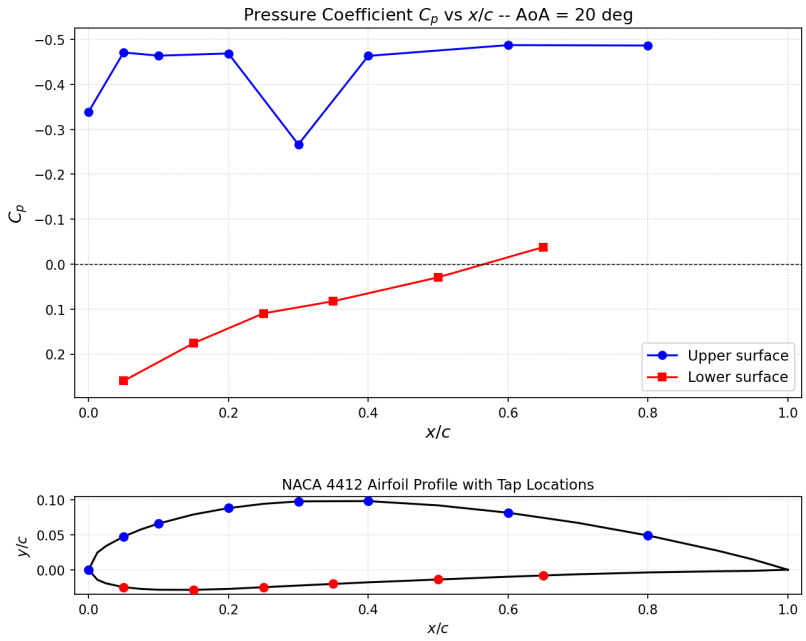

Figure 4.2.21: Pressure Coefficient C_p vs. Non-Dimensional Distance x/c for 20° Angle of Attack

4.3 Pressure Drag and Lift Force

Table 4.3.1: Pressure Drag and Lift Force vs. Angle of Attack

`./outputs/text/flow_and_forces_table.csv`

AoA [°]	L [N/m]	D [N/m]
-20.0	-30.4229	4.5475
-18.0	-26.0501	2.1624
-16.0	-20.4381	-0.3711
-14.0	-17.8976	-1.3563
-12.0	-17.4217	-1.9958
-10.0	-22.5526	-1.3636
-8.0	-28.8415	-0.6819
-6.0	-1.9503	-2.6622
-4.0	17.9793	-3.7719
-2.0	33.9196	-2.328
0.0	44.6257	0.6409
2.0	64.1404	5.4708
4.0	75.6909	12.6457
6.0	93.9975	21.5335
8.0	97.7232	28.6329
10.0	95.1935	34.3285
12.0	90.2319	38.9875
14.0	89.0435	43.861
16.0	63.7691	20.9408
18.0	64.9783	24.2453
20.0	67.5477	28.1179

4.4 Coefficient of Lift

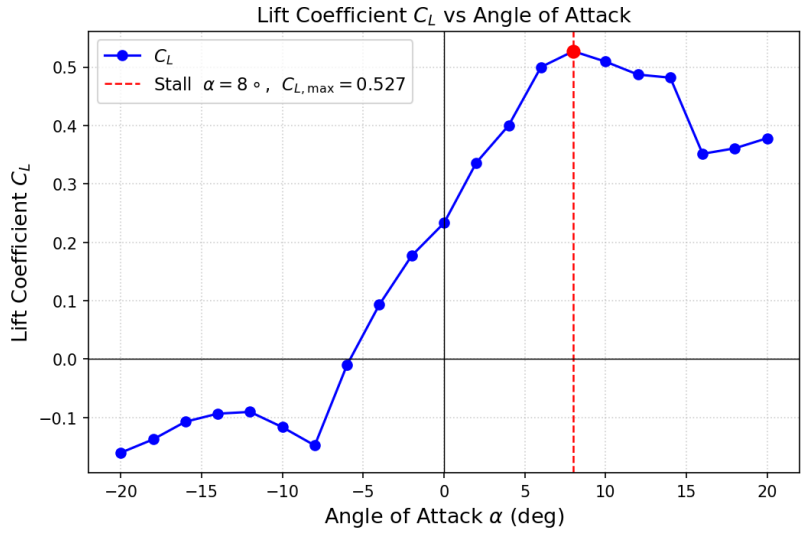

Figure 4.4.1: Lift Coefficient C_L vs. Angle of Attack

Stall is identified as the angle of attack at which C_L reaches its maximum before the onset of flow separation (the first peak when scanning from low to high AoA, i.e. considering only AoA >= 0 to avoid the negative-alpha peak).
From Fig 4.4.1, the estimated stall angle is:

$$\alpha = 8\,^\circ$$

Similarly, the experimental $C_{L,\max}$ is:

$$C_{L,\max} = 0.527086$$

4.5 Coefficient of Drag

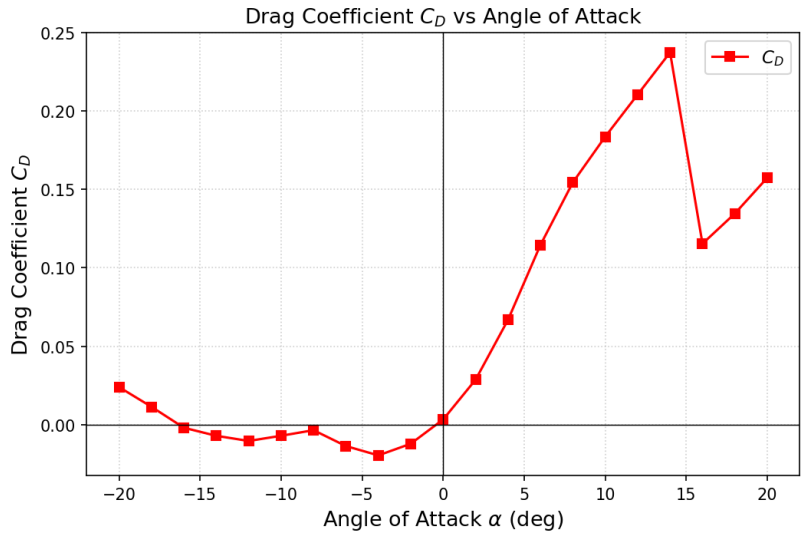

Figure 4.5.1: Drag Coefficient C_D vs. Angle of Attack

5 Analysis and Discussion

5.1 Experimental Aerodynamic Characteristics vs. Published NACA Data

Table 5.1.1 summarises the key aerodynamic characteristics obtained from the experiment alongside the reference values from the published XFoil polar for the NACA 4412 at $Re = 1 \times 10^6$.

Quantity	**Experimental**	**XFoil ($Re = 1 \times 10^6$)**
Maximum C_L	0.527	1.671
Stall angle α_s	8°	16.25°
Zero-lift angle α_0	-5.81°	-4.35°

Table 5.1.1: Comparison of experimental and published aerodynamic characteristics for the NACA 4412 airfoil.

The experimental $C_{L,\max}$ of 0.527 is substantially lower than the XFoil prediction of 1.671, and stall is observed at 8° rather than the predicted 16.25°. Several factors contribute to these discrepancies.
First, the experiment was conducted at $Re \approx 6.58 \times 10^5$, whereas the reference polar is computed at $Re = 1 \times 10^6$. The lower Reynolds number causes the laminar separation bubble to grow more aggressively with increasing angle of attack, advancing the onset of leading-edge stall to a lower angle and reducing the peak lift that can be sustained before separation.
Second, the experimental lift coefficient is derived exclusively from surface pressure integration (Equation 3.2.3), which captures only the normal and axial pressure forces. Any viscous contribution to lift — which is small but non-negligible near stall — is absent from the measurement.
Third, the limited spatial resolution of fourteen pressure taps means that the steep suction peak near the leading edge on the upper surface is poorly resolved at high angles of attack. The trapezoidal integration consequently underestimates the true normal force coefficient, leading to a reduced $C_{L,\max}$ and an apparently earlier stall. The zero-lift angle of -5.81° is in reasonable agreement with the XFoil value of -4.35° and the theoretical expectation of approximately -4° for a 4 % cambered airfoil, suggesting that the pressure measurement technique is reliable in attached-flow conditions.

5.2 Experimental Lift Curve vs. Published NACA Data

The lift curve slope $a_0 = \mathrm{d}C_L/\mathrm{d}\alpha$ was computed by fitting a linear regression to the attached-flow region of each dataset ($-4^\circ \leq \alpha \leq 6^\circ$). The results are compared with two-dimensional thin-aerofoil theory in Table 5.2.1.

Source	a_0 **(per deg)**	a_0 **(per rad)**
Experimental	0.0401	2.30
XFoil ($Re = 1 \times 10^6$)	0.1094	6.27
Thin-aerofoil theory	0.0349	$2\pi \approx 6.28$

Table 5.2.1: Lift curve slope comparison. The XFoil value agrees closely with thin-aerofoil theory; the experimental slope is significantly lower.

The XFoil lift curve slope of $0.1094\,^{\circ -1}$ ($6.27\,\mathrm{rad}^{-1}$) agrees almost exactly with the thin-aerofoil theory prediction of $2\pi \approx 6.28\,\mathrm{rad}^{-1}$, as expected for a well-resolved two-dimensional computation on a smooth airfoil. The experimental slope of $0.0401\,^{\circ -1}$ ($2.30\,\mathrm{rad}^{-1}$) is approximately 37 % of the theoretical value, which is a significant deficit.
The most probable cause is the coarse spatial distribution of the pressure taps. With only eight taps on the upper surface and six on the lower, the trapezoidal integration misses a large fraction of the suction peak

that concentrates near the leading edge ($x/c \lesssim 0.05$) as the angle of attack increases. Since lift is dominated by this leading-edge suction, the integrated C_L grows more slowly with α than the true value, flattening the lift curve. This effect is compounded by three-dimensional tunnel effects (wall interference, finite aspect ratio corrections) and any small misalignment between the model chord line and the prescribed angle of attack. Despite the quantitative discrepancy, the qualitative behaviour is physically consistent: the lift curve is linear over the attached-flow regime, the zero-lift angle is in the correct range for a positively cambered airfoil, and the curve peaks and then falls at high angle of attack in a manner recognisable as leading-edge stall.

5.3 Experimental Drag Polar vs. Published NACA Data

Table 5.3.1 compares the experimental pressure drag coefficient with both the total drag coefficient (C_d) and the pressure drag coefficient ($C_{d,p}$) reported by XFoil at matched angles of attack.

α (deg)	Exp. C_D	XFoil $C_{d,p}$	XFoil C_d (total)
0	0.0033	0.001 41	0.006 78
2	0.0287	0.001 92	0.006 22
4	0.0668	0.002 60	0.007 22
6	0.1145	0.003 79	0.008 84
8	0.1544	0.006 72	0.012 88
10	0.1836	0.010 91	0.017 46

Table 5.3.1: Drag coefficient comparison at positive angles of attack. The XFoil total drag C_d includes both pressure and skin-friction contributions; $C_{d,p}$ is the pressure drag component only.

At $\alpha = 0°$, the experimental C_D of 0.0033 is larger than the XFoil pressure drag of 0.001 41 but smaller than the XFoil total drag of 0.006 78. This is physically consistent: skin friction (approximately 0.004 48 at $\alpha = 0°$) is not captured by the surface pressure taps, so the experimental result should lie between the two XFoil bounds in the attached-flow regime, which it does.

At positive angles above 2°, however, the experimental C_D grows far more rapidly than either XFoil prediction, reaching 0.1836 at $\alpha = 10°$ compared to a total XFoil drag of only 0.017 46. This divergence is consistent with the prematurely low stall angle identified in Section 5.1: once the flow is separating over the upper surface — which the data suggests begins as early as $\alpha \approx 8°$ for this experiment — the pressure on the upper surface downstream of the separation point rises toward the freestream value, greatly increasing the pressure drag component. The XFoil simulation, which remains attached to 16°, does not capture this effect.

At low angles of attack ($-4° \leq \alpha \leq 4°$), both polars show the characteristic low-drag bucket of a well-designed airfoil, and the trends agree qualitatively. The quantitative offset is attributable to the absence of skin friction in the experimental measurement and to the resolution limitations discussed above. Overall, while the absolute magnitudes differ substantially, the experiment correctly captures the rapid drag rise associated with flow separation, which is the most aerodynamically significant feature of the drag polar in a practical context.

6 Summary and Conclusions

This experiment investigated the pressure distribution, lift, and pressure drag on a NACA 4412 airfoil model in a low-speed wind tunnel at $Re \approx 6.58 \times 10^5$. Surface pressures were measured at fourteen tap locations across $-20° \leq \alpha \leq 20°$ and integrated numerically to yield aerodynamic force coefficients. The principal findings are as follows.

Freestream conditions. The mean dynamic pressure derived from the pitot-static system was $q_\infty = 629.15\,\text{Pa}$, consistent to within 3 % across all angles of attack, confirming a stable tunnel speed of $U_\infty = 32.05\,\text{m/s}$ and a chord Reynolds number of $Re = 6.58 \times 10^5$.
Pressure distributions. The C_p distributions behaved as expected for a cambered airfoil in the attached-flow regime: the upper surface exhibited a broad suction region that intensified and migrated toward the leading edge with increasing incidence, while the lower surface remained near or above freestream pressure. At angles of attack beyond $\alpha \approx 8°$, the upper-surface suction collapsed abruptly, consistent with the onset of leading-edge flow separation.
Lift and stall. The experimental lift curve was approximately linear in the range $-4° \leq \alpha \leq 6°$, with a slope of $0.040\,°^{-1}$. The maximum lift coefficient was $C_{L,\max} = 0.527$, reached at $\alpha_s = 8°$. Both values are substantially below the XFoil prediction of $C_{L,\max} = 1.671$ at $\alpha_s = 16.25°$. The deficit is attributed to the inability of the coarse tap array to resolve the narrow leading-edge suction peak, which causes the trapezoidal integration to underestimate the true normal force, and to the lower experimental Reynolds number, which promotes earlier laminar separation relative to the $Re = 1 \times 10^6$ reference polar.
Drag polar. The experimental pressure drag coefficient was physically consistent at low incidence: at $\alpha = 0°$ it fell between the XFoil pressure-only drag (0.001 41) and total drag (0.006 78), as expected given that skin friction is not captured by surface pressure taps alone. Above $\alpha \approx 2°$, the experimental C_D rose far more steeply than the XFoil prediction — reaching 0.184 at $\alpha = 10°$ against an XFoil total of 0.017 — consistent with premature pressure-drag rise due to early flow separation on the upper surface.
Broader considerations. The experiment demonstrates that pressure-tap integration is a reliable technique for estimating aerodynamic forces under attached-flow conditions, but that its accuracy degrades significantly near and beyond stall, where flow separation produces large pressure gradients between taps that the trapezoidal rule cannot faithfully capture. Future work should consider a denser tap distribution near the leading edge ($x/c < 0.05$) to improve resolution of the suction peak, and a direct force balance measurement to provide an independent check on the pressure-integrated results and to recover the skin-friction contribution to drag. Measurements at a Reynolds number closer to 1×10^6 would also reduce the discrepancy with the published polar and allow a more direct validation of the XFoil prediction.

7 References

[1] M. S. Selig, *UIUC airfoil data site*, University of Illinois at Urbana-Champaign: Department of Aeronautical and Astronautical Engineering. [Online]. Available: https://m-selig.ae.illinois.edu/ads/coord_database.html (see pp. 1, 22).

[2] M. Drela and H. Youngren, *XFOIL, Subsonic airfoil development system*, Massachusetts Institute of Technology: Department of Aeronautics and Astronautics. [Online]. Available: https://web.mit.edu/drela/Public/web/xfoil (see p. 23).

[3] J. D. Anderson and C. P. Cadou, *Fundamentals of Aerodynamics*, 7th ed. McGraw-Hill Education, March 17, 2023, ISBN: 9781266076442.

8 Appendices

8.1 Data

Table 8.1.1: Raw Measurements of Pressure Taps vs. Angle of Attack

`./data/pressure_taps_vs_aoa.csv`

```
AoA, Channel 1, Channel 2, Channel 3, Channel 4, Channel 5, Channel 6, Channel 7, Channel 8, Channel 9, Channel 10, Channel 11, Channel 12, Channel 13, Channel 14, Channel 15, Channel 16
-20, -69.206436, -886.344971, -851.163147, -788.391968, -639.438721, -674.0448, -545.104919, -455.617615, -817.457642, -919.410156, -917.260193, -931.250916, -915.066284, -917.640259, -924.629456, -701.653625
-18, -69.603416, -882.826111, -854.786499, -802.204224, -657.729126, -692.203796, -564.708801, -474.265839, -769.434509, -917.917847, -909.879089, -919.090088, -900.592102, -895.604675, -912.701416, -701.046265
-16, -69.735741, -876.179016, -865.009338, -825.352478, -684.256409, -727.949585, -600.341919, -502.057648, -688.143372, -895.648071, -892.579407, -907.257996, -891.658875, -885.664734, -900.205261, -704.690308
-14, -69.471085, -861.451416, -855.433472, -827.526611, -692.366272, -740.803284, -627.09552, -526.480774, -650.031555, -877.166443, -872.281311, -894.111145, -872.887756, -882.670776, -890.435547, -707.48407
-12, -69.471085, -852.849426, -857.245178, -835.967346, -704.826782, -763.572937, -647.04541, -549.219543, -604.146973, -883.480042, -887.158936, -896.302307, -884.421753, -886.622742, -881.006714, -711.249634
-10, -69.868073, -827.043518, -840.810913, -837.118408, -712.206299, -769.693848, -658.807739, -561.731873, -602.893311, -905.29071, -914.146301, -929.717102, -914.387939, -905.664368, -881.1203, -714.164734
-8, -69.338768, -781.817993, -810.918762, -817.423279, -696.600464, -768.714478, -663.881714, -566.544373, -611.9198, -958.669312, -951.052124, -956.01062, -924.338806, -893.449097, -836.36145, -719.266479
-6, -69.338768, -790.680664, -823.341492, -839.164673, -725.997559, -803.113708, -703.976379, -602.036072, -647.022705, -1142.911865, -838.143433, -806.465759, -767.384766, -740.996155, -722.64679, -720.359741
-4, -69.603416, -825.349243, -855.562866, -885.972595, -781.283508, -876.196716, -790.948059, -697.061523, -480.65976, -887.038574, -841.026672, -762.204834, -737.758057, -715.248047, -699.358582, -712.342773
-2, -69.471085, -854.283081, -871.738403, -919.991577, -820.11676, -933.855286, -876.999329, -807.10968, -429.760468, -809.553406, -758.565247, -743.251526, -717.969238, -698.122498, -689.475281, -708.33429
0, -68.941788, -794.851318, -898.654114, -947.871765, -857.740173, -984.53595, -945.909546, -900.596619, -435.276642, -753.534546, -724.081421, -721.230591, -701.911987, -687.940369, -683.784668, -707.605469
2, -69.868073, -797.197266, -958.438477, -983.297546, -902.622131, -1055.6604, -1054.969238, -1045.087402, -504.855743, -681.313965, -675.723755, -686.276245, -673.832764, -671.492249, -670.5802, -705.540527
4, -68.941788, -809.448608, -891.019409, -1026.268799, -939.76178, -1119.562134, -1155.515869, -1196.658569, -669.588928, -619.42865, -636.410645, -653.779358, -648.443604, -651.80249, -659.993896, -699.588623
6, -68.941788, -813.879883, -915.864807, -1088.807495, -996.257446, -1185.055298, -1265.725952, -1365.631226, -924.884216, -566.630554, -601.606934, -625.125061, -625.207947, -634.273804, -647.244873, -695.5802
8, -68.941788, -799.803955, -917.417725, -1053.765259, -1006.298462, -1205.25415, -1351.202271, -1476.511597, -1122.104004, -540.17395, -588.078613, -616.891052, -614.10022, -628.39093, -640.98407, -686.950623
```

```
10, -70.000397, -791.592957, -874.455811, -1023.199463, -995.047668, -1213.700806,
↪  -1282.292114, -1607.751831, -1283.931763, -523.724915, -569.000183, -606.680969,
↪  -605.599365, -629.591492, -653.050232, -693.150818
12, -69.471085, -817.398987, -834.08197, -963.218689, -949.802673, -1197.052124,
↪  -1260.434082, -1714.813354, -1443.235474, -510.036499, -557.784363, -593.067383,
↪  -604.692627, -629.951721, -649.749146, -686.950623
14, -68.941788, -844.768799, -861.386108, -906.051514, -886.411438, -1153.594116,
↪  -1284.937988, -1806.476929, -1602.182495, -494.852722, -553.04364, -587.578064,
↪  -596.985168, -623.588562, -656.123657, -685.002258
16, -69.338768, -956.724792, -965.296875, -949.022766, -818.181091, -957.359375,
↪  -949.360779, -949.920288, -788.693726, -551.216736, -592.24115, -626.881653,
↪  -633.028748, -658.405762, -697.313782, -674.164001
18, -69.471085, -976.926514, -956.368042, -943.523499, -821.326416, -961.521606,
↪  -957.413757, -954.240601, -830.088745, -527.06073, -574.897156, -610.08429, -617.727173,
↪  -658.16571, -696.177734, -669.658203
20, -69.338768, -970.670471, -971.249451, -956.184692, -832.214233, -959.562866,
↪  -956.493286, -960.96106, -877.986633, -501.294342, -554.084229, -595.812073,
↪  -612.853455, -646.279785, -688.565552, -664.665283
```

Table 8.1.2: NACA 4412 Airfoil Coordinates and the Corresponding Tap Locations on the Model Airfoil [1]

`./data/naca_4412_airfoil_coords_and_taps.csv`

x/c	y/c	Tap #	DSA Channel #
1	0	–	01
0.95	0.0147	–	–
0.90	0.0271	–	–
0.80	0.0489	01	02
0.70	0.0669	–	–
0.60	0.0814	02	03
0.50	0.0919	–	–
0.40	0.0980	03	04
0.30	0.0976	04	05
0.25	0.0941	–	–
0.20	0.0880	05	06
0.15	0.0789	–	–
0.10	0.0659	06	07
0.075	0.0576	–	–
0.05	0.0473	07	08
0.025	0.0339	–	–
0.0125	0.0244	–	–
0	0	08	09
0.0125	-0.0143	–	–
0.025	-0.0195	–	–
0.05	-0.0249	09	10
0.075	-0.0274	–	–
0.10	-0.0286	–	–
0.15	-0.0288	10	11
0.20	-0.0274	–	–
0.25	-0.0250	11	12
0.30	-0.0226	–	–
0.35	-0.0203	12	13
0.40	-0.0180	–	–
0.50	-0.0140	13	14
0.60	-0.0100	–	–
0.65	-0.00825	14	15
0.70	-0.0065	–	–
0.80	-0.0039	–	–
0.90	-0.0022	–	–
0.95	-0.0016	–	–
1	0	–	16

Table 8.1.3: NACA 4412 Airfoil Drag Polar [2]

`./data/xf-naca4412-il-1000000.csv`

```
Xfoil polar. Reynolds number fixed. Mach  number fixed
Polar key,xf-naca4412-il-1000000
Airfoil,naca4412-il
Reynolds number,1000000
Ncrit,9
Mach,0
Max Cl/Cd,129.373
Max Cl/Cd alpha,5.25
Url,http://www.airfoiltools.com/polar/csv?polar=xf-naca4412-il-1000000
```

α	C_l	C_d	C_{dp}	C_m	Top_{Xtr}	Bot_{Xtr}
-15.750	-0.8374	0.08373	0.08141	-0.0585	1.0000	0.0169
-15.500	-0.9127	0.06837	0.06591	-0.0687	1.0000	0.0166
-15.250	-1.0965	0.03328	0.03022	-0.0993	1.0000	0.0153
-15.000	-1.1161	0.03120	0.02803	-0.0956	1.0000	0.0154
-14.750	-1.1210	0.02977	0.02651	-0.0926	1.0000	0.0156
-14.500	-1.1215	0.02857	0.02523	-0.0896	1.0000	0.0159
-14.250	-1.1181	0.02751	0.02407	-0.0870	1.0000	0.0162
-14.000	-1.0990	0.02637	0.02282	-0.0871	0.9992	0.0166
-13.750	-1.0711	0.02533	0.02165	-0.0885	0.9979	0.0170
-13.500	-1.0462	0.02365	0.01985	-0.0903	0.9963	0.0177
-13.250	-1.0163	0.02288	0.01905	-0.0918	0.9951	0.0183
-13.000	-0.9847	0.02237	0.01850	-0.0933	0.9943	0.0189
-12.750	-0.9549	0.02183	0.01790	-0.0943	0.9930	0.0195
-12.500	-0.9260	0.02126	0.01724	-0.0952	0.9911	0.0201
-12.250	-0.8954	0.02078	0.01666	-0.0963	0.9894	0.0206
-12.000	-0.8682	0.01946	0.01525	-0.0976	0.9877	0.0214
-11.750	-0.8365	0.01894	0.01471	-0.0990	0.9866	0.0220
-11.500	-0.8038	0.01852	0.01424	-0.1004	0.9857	0.0227
-11.250	-0.7707	0.01808	0.01375	-0.1019	0.9849	0.0235
-11.000	-0.7369	0.01769	0.01328	-0.1035	0.9843	0.0242
-10.750	-0.7070	0.01745	0.01297	-0.1041	0.9819	0.0246
-10.500	-0.6803	0.01619	0.01161	-0.1049	0.9793	0.0257
-10.250	-0.6491	0.01569	0.01109	-0.1060	0.9775	0.0264
-10.000	-0.6172	0.01529	0.01065	-0.1071	0.9759	0.0271
-9.750	-0.5850	0.01491	0.01022	-0.1082	0.9742	0.0279
-9.500	-0.5547	0.01456	0.00981	-0.1089	0.9718	0.0287
-9.250	-0.5287	0.01426	0.00944	-0.1085	0.9665	0.0292
-9.000	-0.5023	0.01345	0.00855	-0.1085	0.9622	0.0299
-8.750	-0.4769	0.01285	0.00791	-0.1082	0.9574	0.0309
-8.500	-0.4513	0.01249	0.00752	-0.1078	0.9519	0.0317
-8.250	-0.4243	0.01214	0.00713	-0.1076	0.9474	0.0324

-8.000	-0.3979	0.01184	0.00678	-0.1073	0.9422	0.0333
-7.750	-0.3715	0.01155	0.00644	-0.1070	0.9363	0.0340
-7.500	-0.3442	0.01127	0.00609	-0.1068	0.9313	0.0345
-7.250	-0.3183	0.01080	0.00556	-0.1064	0.9249	0.0354
-7.000	-0.2921	0.01033	0.00505	-0.1061	0.9186	0.0365
-6.750	-0.2649	0.01003	0.00471	-0.1059	0.9125	0.0375
-6.500	-0.2377	0.00977	0.00441	-0.1057	0.9053	0.0384
-6.000	-0.1825	0.00935	0.00389	-0.1054	0.8910	0.0404
-5.750	-0.1549	0.00912	0.00360	-0.1052	0.8835	0.0414
-5.500	-0.1275	0.00880	0.00325	-0.1051	0.8751	0.0435
-5.000	-0.0718	0.00845	0.00283	-0.1049	0.8578	0.0476
-4.750	-0.0441	0.00824	0.00259	-0.1047	0.8488	0.0519
-4.500	-0.0162	0.00810	0.00243	-0.1046	0.8388	0.0569
-4.250	0.0117	0.00793	0.00228	-0.1045	0.8288	0.0655
-4.000	0.0394	0.00780	0.00213	-0.1044	0.8184	0.0745
-3.750	0.0674	0.00769	0.00201	-0.1044	0.8073	0.0820
-3.500	0.0954	0.00761	0.00191	-0.1043	0.7964	0.0890
-3.250	0.1232	0.00752	0.00180	-0.1042	0.7851	0.0977
-3.000	0.1512	0.00745	0.00171	-0.1041	0.7733	0.1066
-2.750	0.1791	0.00737	0.00163	-0.1040	0.7616	0.1182
-2.500	0.2069	0.00729	0.00156	-0.1040	0.7497	0.1332
-2.250	0.2346	0.00723	0.00150	-0.1039	0.7378	0.1502
-2.000	0.2625	0.00715	0.00145	-0.1038	0.7254	0.1697
-1.750	0.2903	0.00709	0.00142	-0.1038	0.7132	0.1927
-1.500	0.3180	0.00703	0.00141	-0.1037	0.7012	0.2214
-1.250	0.3456	0.00701	0.00139	-0.1036	0.6886	0.2466
-1.000	0.3734	0.00697	0.00138	-0.1035	0.6754	0.2686
-0.750	0.4012	0.00694	0.00137	-0.1035	0.6626	0.2903
-0.500	0.4288	0.00691	0.00138	-0.1034	0.6497	0.3203
-0.250	0.4562	0.00686	0.00139	-0.1033	0.6365	0.3629
0.000	0.4833	0.00678	0.00141	-0.1032	0.6232	0.4192
0.250	0.5102	0.00658	0.00146	-0.1031	0.6101	0.5177
0.500	0.5366	0.00635	0.00153	-0.1029	0.5975	0.6393
0.750	0.5622	0.00617	0.00160	-0.1024	0.5856	0.7449
1.000	0.5842	0.00594	0.00170	-0.1009	0.5740	0.8717
1.250	0.6163	0.00588	0.00177	-0.1014	0.5622	0.9842
1.500	0.6525	0.00598	0.00181	-0.1033	0.5505	1.0000
1.750	0.6788	0.00611	0.00186	-0.1029	0.5398	1.0000
2.000	0.7055	0.00622	0.00192	-0.1026	0.5294	1.0000
2.250	0.7325	0.00633	0.00199	-0.1024	0.5204	1.0000
2.500	0.7592	0.00646	0.00206	-0.1022	0.5112	1.0000
2.750	0.7865	0.00656	0.00213	-0.1020	0.5029	1.0000
3.250	0.8405	0.00681	0.00231	-0.1016	0.4847	1.0000
3.500	0.8672	0.00696	0.00240	-0.1014	0.4746	1.0000
3.750	0.8941	0.00709	0.00250	-0.1012	0.4646	1.0000
4.000	0.9210	0.00722	0.00260	-0.1010	0.4540	1.0000
4.250	0.9473	0.00739	0.00272	-0.1007	0.4426	1.0000

4.500	0.9734	0.00758	0.00284	-0.1004	0.4273	1.0000
4.750	0.9993	0.00778	0.00297	-0.1001	0.4110	1.0000
5.000	1.0254	0.00797	0.00311	-0.0998	0.3979	1.0000
5.250	1.0518	0.00813	0.00326	-0.0995	0.3861	1.0000
5.500	1.0777	0.00834	0.00342	-0.0992	0.3731	1.0000
5.750	1.1031	0.00857	0.00359	-0.0988	0.3575	1.0000
6.000	1.1280	0.00884	0.00379	-0.0983	0.3398	1.0000
6.250	1.1523	0.00914	0.00401	-0.0978	0.3207	1.0000
6.500	1.1761	0.00948	0.00426	-0.0971	0.2993	1.0000
6.750	1.1988	0.00989	0.00455	-0.0963	0.2737	1.0000
7.000	1.2208	0.01036	0.00488	-0.0954	0.2461	1.0000
7.250	1.2417	0.01089	0.00526	-0.0943	0.2173	1.0000
7.500	1.2614	0.01149	0.00569	-0.0931	0.1865	1.0000
7.750	1.2793	0.01220	0.00621	-0.0915	0.1526	1.0000
8.000	1.2973	0.01288	0.00672	-0.0900	0.1252	1.0000
8.250	1.3164	0.01345	0.00719	-0.0887	0.1065	1.0000
8.500	1.3346	0.01404	0.00769	-0.0872	0.0893	1.0000
8.750	1.3514	0.01469	0.00823	-0.0854	0.0729	1.0000
9.000	1.3676	0.01527	0.00875	-0.0836	0.0622	1.0000
9.250	1.3835	0.01581	0.00926	-0.0817	0.0563	1.0000
9.500	1.4004	0.01631	0.00976	-0.0799	0.0521	1.0000
9.750	1.4171	0.01682	0.01028	-0.0782	0.0491	1.0000
10.000	1.4317	0.01746	0.01091	-0.0762	0.0459	1.0000
10.250	1.4484	0.01797	0.01147	-0.0746	0.0442	1.0000
10.500	1.4653	0.01849	0.01203	-0.0731	0.0427	1.0000
10.750	1.4805	0.01911	0.01267	-0.0714	0.0411	1.0000
11.000	1.4938	0.01986	0.01343	-0.0695	0.0392	1.0000
11.250	1.5061	0.02069	0.01430	-0.0676	0.0376	1.0000
11.500	1.5221	0.02129	0.01495	-0.0662	0.0368	1.0000
11.750	1.5369	0.02199	0.01570	-0.0647	0.0356	1.0000
12.000	1.5500	0.02282	0.01656	-0.0631	0.0343	1.0000
12.250	1.5608	0.02382	0.01758	-0.0614	0.0330	1.0000
12.500	1.5688	0.02506	0.01888	-0.0594	0.0316	1.0000
12.750	1.5831	0.02588	0.01975	-0.0582	0.0308	1.0000
13.000	1.5959	0.02683	0.02075	-0.0569	0.0298	1.0000
13.250	1.6066	0.02796	0.02192	-0.0555	0.0286	1.0000
13.500	1.6141	0.02939	0.02338	-0.0540	0.0273	1.0000
13.750	1.6213	0.03089	0.02494	-0.0526	0.0262	1.0000
14.000	1.6325	0.03209	0.02620	-0.0516	0.0252	1.0000
14.250	1.6414	0.03354	0.02770	-0.0505	0.0241	1.0000
14.500	1.6474	0.03528	0.02947	-0.0493	0.0229	1.0000
14.750	1.6508	0.03731	0.03156	-0.0482	0.0218	1.0000
15.000	1.6585	0.03899	0.03332	-0.0474	0.0209	1.0000
15.250	1.6638	0.04096	0.03533	-0.0466	0.0198	1.0000
15.500	1.6661	0.04330	0.03772	-0.0458	0.0187	1.0000
15.750	1.6666	0.04589	0.04037	-0.0451	0.0179	1.0000
16.000	1.6698	0.04827	0.04284	-0.0447	0.0171	1.0000

16.250	1.6706	0.05099	0.04562	-0.0443	0.0164	1.0000
16.500	1.6692	0.05402	0.04871	-0.0440	0.0157	1.0000
16.750	1.6638	0.05759	0.05235	-0.0439	0.0151	1.0000
17.000	1.6605	0.06101	0.05587	-0.0439	0.0146	1.0000
17.250	1.6584	0.06435	0.05931	-0.0441	0.0142	1.0000
17.500	1.6548	0.06793	0.06298	-0.0444	0.0138	1.0000
17.750	1.6497	0.07175	0.06689	-0.0448	0.0134	1.0000
18.000	1.6430	0.07583	0.07106	-0.0453	0.0131	1.0000
18.250	1.6346	0.08024	0.07555	-0.0461	0.0128	1.0000
18.500	1.6237	0.08507	0.08047	-0.0470	0.0124	1.0000
18.750	1.6097	0.09040	0.08590	-0.0482	0.0121	1.0000

8.2 Code

For the sake of brevity, only the code files that are key to the analysis are included below. However, in the spirit of completeness, the repository containing the complete data, source code, and notes for this report can be found at github:vaisriv/enae464-lab02.

Listing 8.2.1: Index File
`./src/index.py`

```python
import pandas as pd
import numpy as np
import matplotlib.pyplot as plt
import matplotlib.gridspec as gridspec
import os

# -- File paths ---------------------------------------------------------------
PRESSURE_FILE = os.path.join("data", "pressure_taps_vs_aoa.csv")
COORDS_FILE   = os.path.join("data", "naca_4412_airfoil_coords_and_taps.csv")
OUT_TEXT    = os.path.join("outputs", "text")
OUT_FIGURES = os.path.join("outputs", "figures")
os.makedirs(OUT_TEXT,    exist_ok=True)
os.makedirs(OUT_FIGURES, exist_ok=True)

# -- Load data ----------------------------------------------------------------
df_p = pd.read_csv(PRESSURE_FILE)
df_p.columns = df_p.columns.str.strip()

df_c = pd.read_csv(COORDS_FILE)
df_c.columns = df_c.columns.str.strip()

# -- Parse tap metadata from coords file --------------------------------------
# Channel 1  (x/c=1, first row)  = open to atmosphere  -> P_atm reference
# Channel 16 (x/c=1, last row)   = tunnel static port   -> P_inf for Cp
# Only rows with a real integer Tap # are actual surface taps (Channels 2-15).
# Dropping rows without a Tap # correctly excludes both reference channels.
tap_rows = df_c.copy()
```

```
tap_rows["Tap #"]         = pd.to_numeric(tap_rows["Tap #"],         errors="coerce")
tap_rows["DSA Channel #"] = pd.to_numeric(tap_rows["DSA Channel #"], errors="coerce")
tap_rows = tap_rows.dropna(subset=["Tap #", "DSA Channel #"]).copy()
tap_rows["Tap #"]         = tap_rows["Tap #"].astype(int)
tap_rows["DSA Channel #"] = tap_rows["DSA Channel #"].astype(int)
tap_rows["x/c"]           = tap_rows["x/c"].astype(float)
tap_rows["y/c"]           = tap_rows["y/c"].astype(float)

# Surface classification: y/c ≥ 0 -> upper, y/c < 0 -> lower
# (leading edge tap at x/c=0, y/c=0 is upper by convention)
tap_rows["surface"] = tap_rows["y/c"].apply(lambda y: "upper" if y ≥ 0 else "lower")

# Sort: upper surface nose->trailing, then lower surface nose->trailing
upper = tap_rows[tap_rows["surface"] == "upper"].sort_values("x/c")
lower = tap_rows[tap_rows["surface"] == "lower"].sort_values("x/c")
taps_ordered = pd.concat([upper, lower]).reset_index(drop=True)

# Map channel number -> column name in pressure DataFrame
def ch_col(n):
    return f"Channel {n}"

# -- Flow conditions ------------------------------------------------------
# Channel 16 = tunnel static pressure -> correct P_inf for Cp definition
# Channel 1  = open to atmosphere     -> independent check / P_atm
#
# Dynamic pressure:
#   q_inf = P_stagnation - P_inf
#   At AoA = 0 the leading-edge tap (Tap 8, Channel 9) is at the stagnation
#   point, so P_stag ~ Channel 9 at AoA=0. Tunnel speed is fixed -> q_inf constant.
#
#   Cp = (P_tap - P_inf) / q_inf   where P_inf = Channel 16

aoa_vals     = df_p["AoA"].values
P_inf_series = df_p[ch_col(16)].values    # tunnel static pressure (Pa gauge)

# q_inf from pitot: Channel 1 (atmosphere) - Channel 16 (tunnel static)
# This is consistent across all AoA (~630 Pa), confirming it is the correct source.
# Use the mean value for Cp normalisation (tunnel speed is nominally constant).
q_inf = (df_p["Channel 1"] - df_p["Channel 16"]).mean()

print(f"Freestream dynamic pressure q_inf (pitot mean) = {q_inf:.2f} Pa")

# -- 1. Build pressures table ---------------------------------------------
pressure_records = []
for _, prow in df_p.iterrows():
    rec = {"AoA": prow["AoA"]}
    for _, trow in taps_ordered.iterrows():
        col_name = f"Tap{int(trow['Tap #'])}_{trow['surface']}_xc{trow['x/c']:.3f}"
```

```
        rec[col_name] = prow[ch_col(int(trow["DSA Channel #"]))]
    pressure_records.append(rec)

df_pressures = pd.DataFrame(pressure_records)
pressure_path = os.path.join(OUT_TEXT, "pressures_table.csv")
df_pressures.to_csv(pressure_path, index=False)
print(f"Saved: {pressure_path}")

# -- 2. Build Cp table ------------------------------------------------------
cp_records = []
for i, prow in df_p.iterrows():
    rec = {"AoA": prow["AoA"]}
    P_inf_i = prow[ch_col(16)]            # tunnel static for this row
    for _, trow in taps_ordered.iterrows():
        P_tap = prow[ch_col(int(trow["DSA Channel #"]))]
        Cp    = (P_tap - P_inf_i) / q_inf
        col_name = f"Cp_Tap{int(trow['Tap #'])}_{trow['surface']}_xc{trow['x/c']:.3f}"
        rec[col_name] = round(Cp, 4)
    cp_records.append(rec)

df_cp = pd.DataFrame(cp_records)
cp_path = os.path.join(OUT_TEXT, "cp_table.csv")
df_cp.to_csv(cp_path, index=False)
print(f"Saved: {cp_path}")


# -- 3. Integrated Cp table (trapezoidal rule) ------------------------------
# Integrate Cp over x/c separately for upper and lower surfaces:
#   C_P_upper = integral of Cp_upper dx/c  from x/c=0 to 1  (leading -> trailing)
#   C_P_lower = integral of Cp_lower dx/c  from x/c=0 to 1
#
# The upper surface Cp is conventionally negative (suction), so C_P_upper will
# be negative; the net normal force coefficient cn = C_P_lower - C_P_upper.
# Both integrals use np.trapz with the tap x/c values as the abscissa.

xc_u_ref = upper["x/c"].values   # fixed tap x/c locations, upper
xc_l_ref = lower["x/c"].values   # fixed tap x/c locations, lower

int_cp_records = []
for i, prow in df_p.iterrows():
    P_inf_i = prow[ch_col(16)]

    cp_u_vals = np.array([
        (prow[ch_col(int(t["DSA Channel #"]))] - P_inf_i) / q_inf
        for _, t in upper.iterrows()
    ])
    cp_l_vals = np.array([
        (prow[ch_col(int(t["DSA Channel #"]))] - P_inf_i) / q_inf
```

```
        for _, t in lower.iterrows()
    ])

    Cp_upper = np.trapezoid(cp_u_vals, xc_u_ref)
    Cp_lower = np.trapezoid(cp_l_vals, xc_l_ref)
    Cn       = Cp_lower - Cp_upper   # net normal force coefficient

    int_cp_records.append({
        "AoA":      prow["AoA"],
        "C_P_upper": round(Cp_upper, 6),
        "C_P_lower": round(Cp_lower, 6),
        "Cn":        round(Cn,       6),
    })

df_int_cp = pd.DataFrame(int_cp_records)
int_cp_path = os.path.join(OUT_TEXT, "integrated_cp_table.csv")
df_int_cp.to_csv(int_cp_path, index=False)
print(f"Saved: {int_cp_path}")


# -- 4. Flow conditions: U_inf and Reynolds number ----------------------------
# Pitot tube reading: q_inf = P_atm - P_static = Channel 1 - Channel 16
#   Channel 1  = atmosphere (total pressure port of pitot)
#   Channel 16 = tunnel static pressure
# This gives a consistent q_inf (~630 Pa) across all AoA, confirming it is
# the correct dynamic pressure source.
#
# Physical constants (standard sea-level air):
RHO     = 1.225       # kg/m^3, air density
MU      = 1.789e-5    # Pa·s,   dynamic viscosity
CHORD   = 0.3         # m,      airfoil chord length (set to your model's chord)
SPAN    = 1.0         # m,      airfoil span (per-unit-span if 1.0)

q_inf_per_aoa = (df_p["Channel 1"] - df_p["Channel 16"]).values   # Pa, one per AoA row
U_inf_per_aoa = np.sqrt(2.0 * q_inf_per_aoa / RHO)                # m/s
Re_per_aoa    = RHO * U_inf_per_aoa * CHORD / MU

# Use the mean q_inf (tunnel speed is nominally constant) for Cp normalisation
q_inf = q_inf_per_aoa.mean()
U_inf = np.sqrt(2.0 * q_inf / RHO)
Re    = RHO * U_inf * CHORD / MU

print(f"\nMean dynamic pressure  q_inf = {q_inf:.2f} Pa")
print(f"Freestream velocity    U_inf = {U_inf:.3f} m/s")
print(f"Reynolds number        Re    = {Re:.4e}  (chord = {CHORD} m)")

# -- 5. Pressure drag and lift at each AoA ------------------------------------
# From the integrated Cp distributions:
```

```
#
#   Normal force coefficient (already computed):
#     Cn = C_P_lower - C_P_upper   (positive = upward)
#
#   Axial (chord-wise) force coefficient via leading-edge pressure distribution.
#   For pressure-only drag, integrate Cp over the airfoil surface projected onto
#   the chord axis.  Using the surface y/c coordinates of the taps:
#
#     Ca = -( integral Cp_upper d(y/c) - integral Cp_lower d(y/c) )
#
#   Then resolve into lift and drag in the wind axis:
#     CL = Cn * cos(alpha) - Ca * sin(alpha)
#     CD = Cn * sin(alpha) + Ca * cos(alpha)
#
#   Forces per unit span:
#     L = CL * q_inf * CHORD * SPAN
#     D = CD * q_inf * CHORD * SPAN

xc_u_ref = upper["x/c"].values
xc_l_ref = lower["x/c"].values
yc_u_ref = upper["y/c"].values
yc_l_ref = lower["y/c"].values

flow_records = []
for i, prow in df_p.iterrows():
    aoa_deg = float(prow["AoA"])
    alpha   = np.radians(aoa_deg)
    q_i     = prow["Channel 1"] - prow["Channel 16"]   # per-AoA dynamic pressure
    U_i     = np.sqrt(2.0 * q_i / RHO)
    Re_i    = RHO * U_i * CHORD / MU

    P_inf_i = prow[ch_col(16)]

    cp_u_vals = np.array([
        (prow[ch_col(int(t["DSA Channel #"]))] - P_inf_i) / q_inf
        for _, t in upper.iterrows()
    ])
    cp_l_vals = np.array([
        (prow[ch_col(int(t["DSA Channel #"]))] - P_inf_i) / q_inf
        for _, t in lower.iterrows()
    ])

    # Normal force coefficient (perpendicular to chord)
    Cn = np.trapezoid(cp_l_vals, xc_l_ref) - np.trapezoid(cp_u_vals, xc_u_ref)

    # Axial force coefficient (along chord, positive toward trailing edge)
    # Upper surface: Cp acts inward (negative y direction) → contributes +Ca
    # Lower surface: Cp acts inward (positive y direction) → contributes -Ca
```

```
    Ca = -(np.trapezoid(cp_u_vals, yc_u_ref) - np.trapezoid(cp_l_vals, yc_l_ref))

    # Wind-axis coefficients
    CL = Cn * np.cos(alpha) - Ca * np.sin(alpha)
    CD = Cn * np.sin(alpha) + Ca * np.cos(alpha)

    # Dimensional forces per unit span (N/m)
    L = CL * q_i * CHORD * SPAN
    D = CD * q_i * CHORD * SPAN

    flow_records.append({
        "AoA (deg)":   aoa_deg,
        "q_inf (Pa)":  round(q_i,    4),
        "U_inf (m/s)": round(U_i,    4),
        "Re":          round(Re_i,   1),
        "Cn":          round(Cn,     6),
        "Ca":          round(Ca,     6),
        "CL":          round(CL,     6),
        "CD":          round(CD,     6),
        "Lift (N/m)":  round(L,      4),
        "Drag (N/m)":  round(D,      4),
    })

df_flow = pd.DataFrame(flow_records)
flow_path = os.path.join(OUT_TEXT, "flow_and_forces_table.csv")
df_flow.to_csv(flow_path, index=False)
print(f"Saved: {flow_path}")

# -- 6. Cp vs x/c plots ------------------------------------------------------
# Full airfoil coordinates for shape subplot
xc_all = df_c["x/c"].astype(float).values
yc_all = df_c["y/c"].astype(float).values

for _, prow in df_p.iterrows():
    aoa     = int(prow["AoA"])
    P_inf_i = prow[ch_col(16)]            # tunnel static for this AoA

    xc_u, cp_u, yc_u_tap = [], [], []
    xc_l, cp_l, yc_l_tap = [], [], []

    for _, trow in taps_ordered.iterrows():
        P_tap = prow[ch_col(int(trow["DSA Channel #"]))]
        Cp    = (P_tap - P_inf_i) / q_inf
        if trow["surface"] == "upper":
            xc_u.append(trow["x/c"])
            cp_u.append(Cp)
            yc_u_tap.append(trow["y/c"])
        else:
```

```
            xc_l.append(trow["x/c"])
            cp_l.append(Cp)
            yc_l_tap.append(trow["y/c"])

    xc_u, cp_u = np.array(xc_u), np.array(cp_u)
    xc_l, cp_l = np.array(xc_l), np.array(cp_l)
    yc_u_tap   = np.array(yc_u_tap)
    yc_l_tap   = np.array(yc_l_tap)

    fig = plt.figure(figsize=(10, 8))
    gs  = gridspec.GridSpec(2, 1, height_ratios=[3, 1], hspace=0.35)

    # Top: Cp plot
    ax1 = fig.add_subplot(gs[0])
    ax1.plot(xc_u, cp_u, "bo-", label="Upper surface", markersize=6)
    ax1.plot(xc_l, cp_l, "rs-", label="Lower surface", markersize=6)
    ax1.axhline(0, color="k", linewidth=0.7, linestyle="--")
    ax1.invert_yaxis()   # convention: Cp decreases upward
    ax1.set_xlim(-0.02, 1.02)
    ax1.set_xlabel(r"$x/c$", fontsize=13)
    ax1.set_ylabel(r"$C_p$", fontsize=13)
    ax1.set_title(rf"Pressure Coefficient $C_p$ vs $x/c$ -- AoA = {aoa} deg", fontsize=13)
    ax1.legend(fontsize=11)
    ax1.grid(True, linestyle=":", alpha=0.6)

    # Bottom: airfoil shape with taps at actual y/c positions
    ax2 = fig.add_subplot(gs[1])
    ax2.plot(xc_all, yc_all, "k-", linewidth=1.5)
    ax2.scatter(xc_u, yc_u_tap, color="blue", s=40, zorder=3, label="Upper taps")
    ax2.scatter(xc_l, yc_l_tap, color="red",  s=40, zorder=3, label="Lower taps")
    ax2.set_xlim(-0.02, 1.02)
    ax2.set_aspect("equal")
    ax2.set_xlabel(r"$x/c$", fontsize=11)
    ax2.set_ylabel(r"$y/c$", fontsize=11)
    ax2.set_title("NACA 4412 Airfoil Profile with Tap Locations", fontsize=11)
    ax2.grid(True, linestyle=":", alpha=0.5)

    fname = os.path.join(OUT_FIGURES, f"cp_vs_xc_AoA_{aoa:+03d}deg.png")
    plt.savefig(fname, dpi=150, bbox_inches="tight")
    plt.close()
    print(f"Saved: {fname}")


# -- 7. CL and CD vs AoA plots + stall estimate ------------------------------
# Pull CL, CD, and AoA directly from the already-computed df_flow.
aoa_plot = df_flow["AoA (deg)"].values
CL_plot  = df_flow["CL"].values
CD_plot  = df_flow["CD"].values
```

```
316
317 # -- Stall estimate ------------------------------------------------------
318 # Stall is identified as the angle of attack at which CL reaches its maximum
319 # before the onset of flow separation (the first peak when scanning from low
320 # to high AoA, i.e. considering only AoA ≥ 0 to avoid the negative-alpha peak).
321 positive_mask  = aoa_plot ≥ 0
322 CL_pos         = CL_plot[positive_mask]
323 aoa_pos        = aoa_plot[positive_mask]
324 stall_idx      = int(np.argmax(CL_pos))
325 CL_max         = CL_pos[stall_idx]
326 aoa_stall      = aoa_pos[stall_idx]
327
328 print(f"\nStall estimate:")
329 print(f"  CL_max   = {CL_max:.4f}")
330 print(f"  AoA_stall = {aoa_stall:.1f} deg")
331
332 # Write stall summary to text file
333 stall_path = os.path.join(OUT_TEXT, "stall_estimate.csv")
334 pd.DataFrame([{"AoA_stall (deg)": aoa_stall, "CL_max": round(CL_max, 6)}]).to_csv(
335     stall_path, index=False
336 )
337 print(f"Saved: {stall_path}")
338
339 # -- Plot: CL vs AoA -----------------------------------------------------
340 fig, ax = plt.subplots(figsize=(8, 5))
341
342 ax.plot(aoa_plot, CL_plot, "bo-", markersize=6, linewidth=1.5, label=r"$C_L$")
343 ax.axvline(aoa_stall, color="red", linestyle="--", linewidth=1.2,
344            label=rf"Stall  $\alpha = {aoa_stall:.0f}\circ$,  $C_{{L,\max}} = {CL_max:.3f}$")
345 ax.scatter([aoa_stall], [CL_max], color="red", zorder=5, s=60)
346
347 ax.set_xlabel(r"Angle of Attack $\alpha$ (deg)", fontsize=13)
348 ax.set_ylabel(r"Lift Coefficient $C_L$", fontsize=13)
349 ax.set_title(r"Lift Coefficient $C_L$ vs Angle of Attack", fontsize=13)
350 ax.legend(fontsize=11)
351 ax.grid(True, linestyle=":", alpha=0.6)
352 ax.axhline(0, color="k", linewidth=0.7)
353 ax.axvline(0, color="k", linewidth=0.7)
354
355 cl_path = os.path.join(OUT_FIGURES, "CL_vs_AoA.png")
356 plt.savefig(cl_path, dpi=150, bbox_inches="tight")
357 plt.close()
358 print(f"Saved: {cl_path}")
359
360 # -- Plot: CD vs AoA -----------------------------------------------------
361 fig, ax = plt.subplots(figsize=(8, 5))
362
363 ax.plot(aoa_plot, CD_plot, "rs-", markersize=6, linewidth=1.5, label=r"$C_D$")
```

```
364
365 ax.set_xlabel(r"Angle of Attack $\alpha$ (deg)", fontsize=13)
366 ax.set_ylabel(r"Drag Coefficient $C_D$", fontsize=13)
367 ax.set_title(r"Drag Coefficient $C_D$ vs Angle of Attack", fontsize=13)
368 ax.legend(fontsize=11)
369 ax.grid(True, linestyle=":", alpha=0.6)
370 ax.axhline(0, color="k", linewidth=0.7)
371 ax.axvline(0, color="k", linewidth=0.7)
372
373 cd_path = os.path.join(OUT_FIGURES, "CD_vs_AoA.png")
374 plt.savefig(cd_path, dpi=150, bbox_inches="tight")
375 plt.close()
376 print(f"Saved: {cd_path}")
377
378 print("\nDone! CSVs -> ./outputs/text/   |   Plots -> ./outputs/figures/")
```